crystals

MDPI

Article

Surface Groups and Dielectric Properties of $Ti_3C_2T_x$ MXene Nanosheets after $NH_3{\cdot}H_2O$ Solvothermal Treatment under Different Temperatures

Zhiwei Liu †, Guanlong Li †, Yan Zhao * and Xiangbao Chen

School of Materials Science and Engineering, Beihang University, Beijing 100191, China; lzwbuaa@163.com (Z.L.); 1601lgl@buaa.edu.cn (G.L.)

* Correspondence: jennyzhaoyan@buaa.edu.cn

† These authors contributed equally to this work.

Abstract: The rapid development of electronic technology has brought convenience and efficiency to the lives of modern people, while emphasizing the need for novel materials with designability and excellent dielectric properties at the same time. In this work, $Ti_3C_2T_x$ MXene nanosheets (MNSs) underwent $NH_3{\cdot}H_2O$ solvothermal treatment at temperatures of 40 °C, 60 °C, 80 °C, 100 °C, 120 °C, 140 °C, 160 °C, and 180 °C. The changes in the surface groups and dielectric properties after the solvothermal treatment were studied. The solvothermal treatment increased the proportion of surface -OH groups, which was beneficial to the permittivity of the MNSs. However, as the treating temperature increased, the amount of -OH on the surface of the MNSs showed a reducing trend, according to XPS spectra. As the treating temperature rose from 40 °C to 80 °C, the real part of the permittivity of MNS sample showed a significant decrease, eventually remaining approximately stable in the 80 °C to 180 °C samples. The results of electromagnetic characterization were in line with the group proportion, as determined via the XPS O1s spectra, supporting the previous conclusion that the -OH group played an important role in the permittivity.

Keywords: $NH_3{\cdot}H_2O$ solvothermal; end groups; dielectric property; 2D nanosheets

check for updates

Citation: Liu, Z.; Li, G.; Zhao, Y.; Chen, X. Surface Groups and Dielectric Properties of $Ti_3C_2T_x$ MXene Nanosheets after $NH_3{\cdot}H_2O$ Solvothermal Treatment under Different Temperatures. *Crystals* **2023**, *13*, 1005. https://doi.org/10.3390/cryst13071005

Academic Editor: Yuri Kivshar

Received: 27 May 2023
Revised: 17 June 2023
Accepted: 21 June 2023
Published: 25 June 2023

Copyright: © 2023 by the authors. Licensee MDPI, Basel, Switzerland. This article is an open access article distributed under the terms and conditions of the Creative Commons Attribution (CC BY) license (https://creativecommons.org/licenses/by/4.0/).

1. Introduction

The rapid development of electronic technology has created an urgent problem with regard to light, small electronic materials. Novel electronic devices such as antennae and supercapacitors that are lightweight, compact in size, and simple to manufacture have been replacing traditional single, large pieces of equipment while necessitating the development and production of light, designable materials with expected dielectric properties [1,2].

Among the materials attracting significant attention with their excellent electronic properties, two-dimensional (2D) materials stand out as nanomaterials with unique properties, especially in the fields of functional materials, such as heat-conduction [3], electricity-conduction [4], supercapacitors [5], and electromagnetic wave absorption [6]. It was not until the discovery of single-layered graphene in 2004 that 2D materials began to receive attention; however, the family of 2D materials has now been substantially and rapidly expanded to include a range of 2D transition metal dichalcogenides [7], layered double hydroxides [8], hexagonal boron nitride [9], transition metal oxides [10], nitrides [11], and MXenes [12].

Two-dimensional transition metal carbides and nitrides, well-known MXenes, have been attracting attention continuously since their discovery in 2013 [13]. MXenes combine high carrier densities and good electricity conductivities similar to graphene with a much better hydrophilicity and designability of surface groups [14]. The most commonly used "top-down" method for the synthesis of MXenes involves the selective etching of the "A"

layers in the MAX phase using a set of Lewis acids, such as HF [13], LiF-HCl [15], transition metal chloride, and bromide [16].

The surface group of MXenes plays an important role in various properties of the nanosheets. The electrical properties, such as conductivity, electron mobility, and dielectric properties, are assumed to be influenced by the categories and amount of the surface group of MXenes, while the chemical characteristics of the surface groups determines the compatibility between MXenes and other solvents, which mainly determines the available synthesis and processing route of MXenes [17]. The surface groups of MXenes etched via HF or LiF-HCl mainly consist of -OH and -F, while the termination of these MXenes can be directionally changed in post-treatment under different temperatures, moisture, atmosphere, or pH [2]. For example, Kamysbayev et al. [16] used a molten salt route to obtain MXene with -Cl and -Br terminations, followed by surface modification to attach =O, =Se, and =Te to the surface of MXene, showing an extraordinary enhancement regarding the superconductivity of MXene. Density functional theory computation was used by Tang et al. [18] to predict that the elimination of surface terminations of MXene enhances its electricity conductivity and provides a small amount of magnetism. As for dielectric properties, Tu et al. [19] reported a rising trend in the dielectric permittivity of the MXene/poly(vinylidene fluoride-trifluoro-ethylene-chlorofluoroehylene) composite as the surface functional groups on the MXene surface (-O, -F, and -OH) increase. Although the connection between surface terminations and dielectric permittivity has been observed, the specific relationship between the post-treatment of LiF-HCl-etched MXene and its dielectric properties is still unclear.

In this work, $Ti_3C_2T_x$ MXene nanosheets (MNSs) underwent $NH_3{\cdot}H_2O$ solvothermal treatment at temperatures of 40 °C, 60 °C, 80 °C, 100 °C, 120 °C, 140 °C, 160 °C, and 180 °C, respectively. Changes in the surface groups and dielectric properties after the solvothermal treatment were studied. The solvothermal treatment increased the proportion of surface -OH groups, which was beneficial to the permittivity of the MNS. As the treating temperature rose from 40 °C to 80 °C, the real part of the permittivity of the MNS sample showed a significant decrease and eventually remained essentially the same within the 80 °C to 180 °C samples. The results of the electromagnetic characterization were in accord with the group proportion, as concluded using XPS O1s spectra, supporting the previous conclusion that the -OH group played an important role in the permittivity.

2. Materials and Methods

2.1. Materials

Titanium aluminum carbide powders (Ti_3AlC_2, 400 mesh, purity of 98%, 11 technology Co., Ltd., Changchun, Jilin, China), hydrochloric acid (HCl, 36–38%, Modern Oriental (Beijing) Technology Development Co., Ltd., Beijing, China), lithium fluoride (LiF, purity of 99%, Shanghai Aladdin Biochemical Technology Co., Ltd., Shanghai, China), ammonium hydroxide solution ($NH_3{\cdot}H_2O$, 25–28%, Shanghai Macklin Biochemical Co., Ltd., Shanghai, China), and paraffin wax were utilized.

2.2. Preparation of $Ti_3C_2T_x$ MXene

$Ti_3C_2T_x$ MXene nanosheets were prepared in line with previous studies. An amount of 1 g of LiF was added to 20 mL of 9M HCl solution and stirred at 0 °C in the ice-water bath for 15 min. Next, 1 g of Ti_3AlC_2 MAX was slowly added to the mixture within 10 min, and the reaction was processed at 45 °C for 45 h. The reaction products were washed with deoxygenated water several times until the pH value was close to 7. Finally, the few-layered $Ti_3C_2T_x$ MXene was obtained via sonication for 60 min under Ar flow to prevent the MXene sheet structure from being oxidized and destroyed. The MXene dispersion obtained via ultrasound was freeze-dried for 72 h in order to obtain dry and pure MXene nanoplate powder.

2.3. Solvothermal Synthesis of $Ti_3C_2T_x$ MXene Nanosheet (MNS)

A total of 1 mol/L $NH_3{\cdot}H_2O$ solution (pH = 11.63) was prepared. A total of 50 mL of $NH_3{\cdot}H_2O$ solution was placed in a tetrafluorylene hydrothermal synthesis reactor, and 150 mg of $Ti_3C_2T_x$ MXene powder was added; then, the mixture was heated to a set of different temperatures (40 °C, 60 °C, 80 °C, 100 °C, 120 °C, 140 °C, 160 °C, and 180 °C), and the temperatures were maintained for 24 h. The products were washed with deoxygenated water until the pH value of the supernatant was close to 7 and then it was freeze-dried for 72 h until dry. The dried powders were collected for subsequent characterization. The collected $NH_3{\cdot}H_2O$-treated MXenes were named MN-1 to MN-8 in an ascending order of treatment temperature.

2.4. Characterization

The microstructure and morphology of the products were characterized using scanning electron microscopy (SEM, JEOL-JSM7500, JEOL, Tokyo, Japan), transmission electron microscopy (TEM, JEOL-JEM2100F, JEOL, Tokyo, Japan), and atom force microscopy (AFM, Bruker-ICON, Bruker, Billericca, Massachusetts, United States). The elemental and structural characterization of the products was carried out via X-ray diffraction (XRD, D/MAX 2500, Rigaku, Tokyo, Japan), X-ray photoelectron spectroscopy (XPS, ESCALab220i-XL, VG Scientific, St. Leonards, Britain), and Raman spectroscopy (LabRAM HR Evolution, HORIBA, Paris, France). The dielectric performances of the MNSs/paraffin composite (mass fraction 30%:70%) in the frequency range of 2–18 GHz were evaluated with a vector network analyzer (CETC AV3672C, Ceyear, Qingdao, Shandong, China).

3. Results and Discussion

3.1. Preparation of $Ti_3C_2T_x$ MXene

$Ti_3C_2T_x$ MXene nanosheets (MNSs) were prepared by etching Ti_3AlC_2 MAX phase. A typical accordion-like morphology can be clearly seen in the SEM image of the sample (Figure 1a), indicating a multi-layered structure which is different from the structure of MAX. After a delaminating process via sonication, the multi-layered MXene tended to transform into few-layered nanosheets. TEM images (Figure 1b) showed that the Mxene nanosheets were semitransparent with organized diffraction patterns, indicating their extremely small thickness and ordered crystal structures. According to the AFM thickness measurement provided in Figure 1c, the thickness of few-layered nanosheets varied between 2 nm to 5 nm. The MNSs dispersed in H_2O showed a typical Tyndall effect (Figure 1d) and remained stable after 48 h, showing colloidal properties.

A comparison between the XRD patterns of MXene and MAX (Figure 1e) confirmed the shifting of the crystal structure after etching. A series of characteristic peaks of MAX disappeared in MXene's pattern, while an obvious position shifting of the (002) peak from 8.7° to 6.5° was observed, indicating the (002) spacing increased after etching. XPS spectra (Figure 1f) showed a disappearing Al 2p peak after etching, proving the elimination of Al atom layers. Moreover, the XPS result indicated that a number of O and F atoms were included in MNSs, primarily showing the composition of the surface functional groups of MNSs.

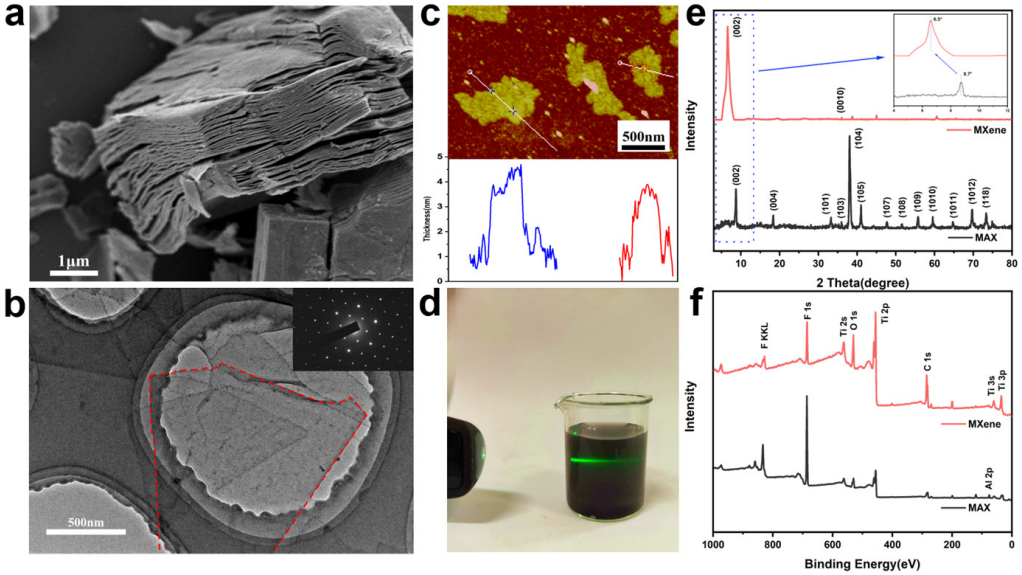


Figure 1. Characterizations of prepared $Ti_3C_2T_x$ Mxene: SEM (**a**), TEM (**b**), and AFM (**c**) images; macrophotography (**d**); and XRD (**e**) and XPS (**f**) spectra compared to MAX. In (**c**), the blue and red curves in the lower image are the sample thickness dimensions of the middle segment of the blue and red dots in the upper image, respectively.

3.2. Solvothermal Treatment

The Ti_3AlC_2 MAX phase was etched through LiF-HCl into $Ti_3C_2T_x$ MXene. The product was subsequently sonicated to form few-layered MXene nanosheets (MNSs), followed by solvothermal treatment in $NH_3 \cdot H_2O$ solution at different temperatures. X-ray diffraction analysis (XRD) was carried out to study the crystal structure of the MNSs after solvothermal treatment, as shown in Figure 2a. A diffraction peak at around 6.6° could be seen in each sample, corresponding to the characteristic peak of (002) crystal plane of $Ti_3C_2T_x$ MXene. No characteristic peak of either anatase phase (25.6° and 47.7°) or rutile phase (26.7°) TiO_2 was observed, indicating that even under high temperature hydrothermal treatment, reductive $NH_3 \cdot H_2O$ prevented MXene from being oxidized to TiO_2. After the solvothermal treatment, Ti atoms in MNSs remained in the layers of Ti, stuck in the alternating structure of Ti and C atom layers, while O atoms were mainly bonded with Ti atoms in the form of O-containing functional groups.

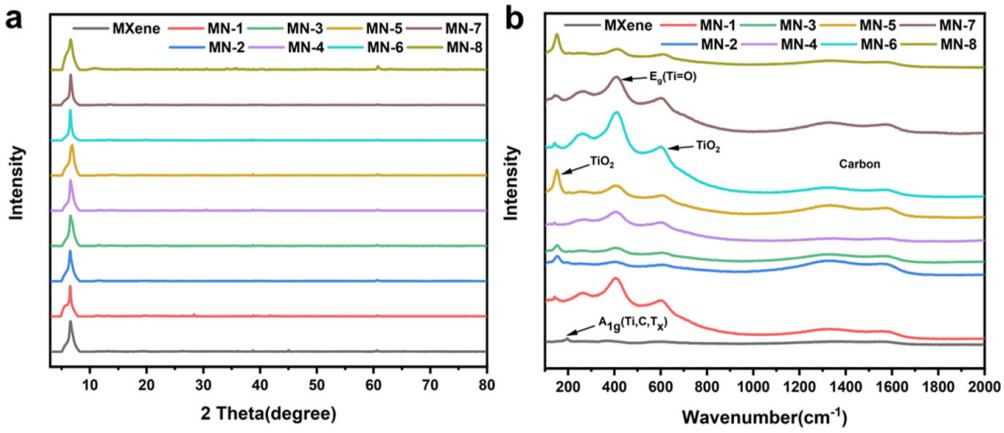


Figure 2. XRD pattern (**a**) and Raman spectra (**b**) of MNS treated with $NH_3 \cdot H_2O$ solution under different temperatures.

It is also worth mentioning that the peak position of (002) peak hardly changed with the increase in treating temperature. The peak position of characteristic peaks of MXene is decided by its crystal plane spacing. Consistent (002) peak positions indicated that the crystal structure of the MNSs was not destroyed by solvothermal treatment, further proving that the Ti atoms had not been oxidized.

Raman spectra under a 633 nm wavelength laser were collected and are shown in Figure 2b. The characteristic peak of $Ti_3C_2T_x$ MXene consists of two parts: E_g (in-plane) and A_{1g} (out-of-plane) peaks, which could both be observed in the samples before and after $NH_3{\cdot}H_2O$ solvothermal treatment, confirming that the main part of MNSs remains $Ti_3C_2T_x$ MXene. The E_g peak of $Ti_3C_2T_x$ MXene at a wavenumber of about 460 cm^{-1} was observed to be obviously intensified after $NH_3{\cdot}H_2O$ solvothermal treatment, which indicated a considerable increase in the oxygen-containing functional groups on the surface of MNSs. At the same time, relatively weak TiO_2 peaks at wavenumbers of around 160 cm^{-1} and 630 cm^{-1} and a slight enhancement of the carbon peaks at 1300~1600 cm^{-1} indicated the very minimal oxidation of the surface Ti atoms of the MNSs, which is consistent with the conclusion from XRD.

X-ray photoelectron spectroscopy (XPS) is widely used in the characterization of the elemental contents of MNS surfaces. The XPS total spectra of the MNS samples after $NH_3{\cdot}H_2O$ solvothermal treatment are provided in Figure 3a. Four main characteristic peaks can be observed in the spectra, corresponding to F 1s, O 1s, Ti 2p, and C 1s, respectively. $Ti_3C_2T_x$ MXene is terminated by various functional groups grafted on Ti atoms. The categories and contents of the terminations are decided by the etching and post-treatment processes. A commonly used LiF-HCl etching route results in a set of terminating groups consisting of -OH, =O, and -F. On the basis of confirming that no TiO_2 was formed, we restricted the surface functional group composition of MNSs after solvothermal treatment into combinations of these three groups with varying proportions.

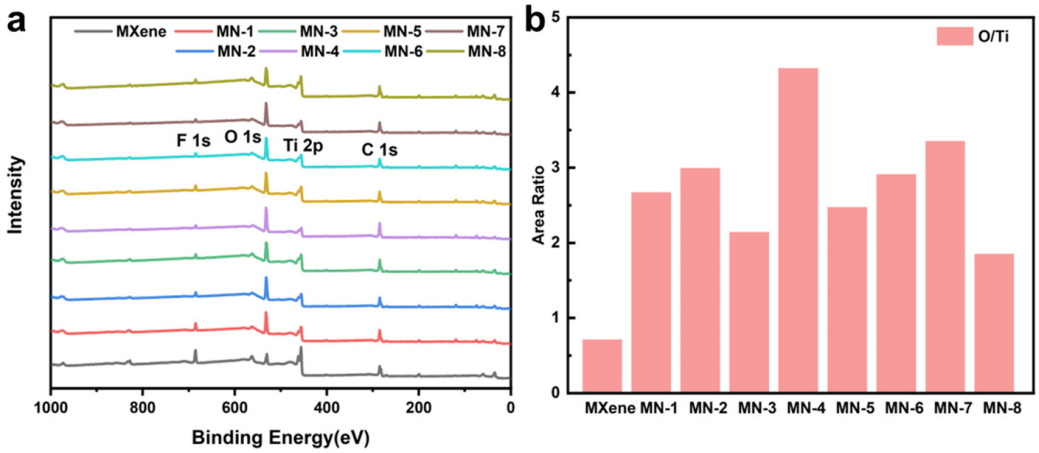


Figure 3. XPS survey spectra (**a**) and O/Ti ratio (**b**) of the MNSs before and after solvothermal treatment.

The quantitative statistics of the atomic proportions, along with O/F and O/Ti atom ratios are provided in Table 1. An obvious decrease in F element from 17.40% of pure MXene was observed after $NH_3{\cdot}H_2O$ solvothermal treatment, and the F proportion generally kept declining as the treating temperature rose. According to previous research [20], -F groups tend to be substituted by oxygen-containing groups in basic environments. This phenomenon was confirmed by the decrease in the F element as well as the O/F ratios. The O/F ratio rose from 1.01 to 3.70~11.70 after the solvothermal treatment, showing a consistent trend with the decline in F proportion. While the decline in the -F functional group could be derived from F proportion and O/F ratio, the increase in O/Ti ratio from 0.71 to 1.85~4.32 indicated an increase in oxygen-containing functional groups (-OH and =O). In conclusion, an obvious substitution of the surface -F groups on MNSs, replaced by oxygen-containing functional groups, occurred after $NH_3{\cdot}H_2O$ solvothermal treatment.

Table 1. XPS statistics of elemental proportions and O/F and O/Ti atom ratios.

Samples	Treating Temperature/°C	Elemental Proportion/%				Atom Ratio	
		C	Ti	O	F	O/F	O/Ti
MXene	-	40.22	24.77	17.61	17.40	1.01	0.71
MN-1	40	39.44	13.80	36.82	9.95	3.70	2.67
MN-2	60	36.97	14.17	42.34	6.52	6.49	2.99
MN-3	80	41.08	16.77	35.94	6.21	5.79	2.14
MN-4	100	47.33	9.14	39.53	4.01	9.86	4.32
MN-5	120	38.19	15.87	39.2	6.74	5.82	2.47
MN-6	140	36.69	14.95	43.55	4.81	9.05	2.91
MN-7	160	41.71	12.56	42.13	3.60	11.70	3.35
MN-8	180	39.15	19.50	36.16	5.19	6.97	1.85

During the $NH_3 \cdot H_2O$ solvothermal treatment, the substitution of fluorine-containing functional groups to oxygen-containing functional groups on the surface of MXene occurred continuously. A suitable temperature played a role of increasing the substitution rate in this process, while temperatures that were too high would reduce the surface functional groups of MXene. The data in Table 1 are plotted and shown in Figure 3b. It can be seen that when the temperature was maintained in a lower range, that is, 40 °C–80 °C, the substitution of fluorine-containing functional groups to oxygen-containing functional groups continued to occur, but at a similar level, with an O/Ti ratio around 2.5. However, when the temperature was raised to 100 °C, the O/Ti ratio rose sharply to 4.32, indicating that the substitution of fluorine-containing functional groups to oxygen-containing functional groups on the MXene surface reached its best effect at this temperature. However, when the temperature was further increased, the temperature played a significant role in the inhibition of MXene surface functional groups, and the O/Ti ratio dropped below 3. When the temperature was raised to 180 °C, the O/Ti ratio dropped below 2, indicating that the surface functional groups of MXene were strongly inhibited by the temperature.

The high resolution XPS analysis of the O 1s peaks of the samples was performed to further study the changes of surface oxygen-containing functional groups of MNSs, and the results are shown in Figure 4. The O 1s peak can be divided into three secondary peaks according to the bonding condition of the O atoms on the surface of MNSs. In addition, the positions and area ratios of O 1s differentiated peaks are provided in Table 2. The area proportion of a differentiated peak to the whole peak represents the amount proportion of the atoms in the bonding situation for which the differentiated peak stands. It could be seen that a significant enlargement of the (C-Ti-$(OH)_x$) peak occurred after $NH_3 \cdot H_2O$ solvothermal treatment, indicating a considerable increase in the amount of -OH groups on the surface of MNSs. The area ratio between the (C-Ti-$(OH)_x$) peak and ((C-Ti-O_x) + (Ti-O)) (see Figure 5a) also supported the conclusion that during the solvothermal treatment, lots of other surface functional groups (mainly -F) were substituted by -OH, resulting in a -OH-rich surface. In the meanwhile, the proportion of the Ti-O peak showed a decline after the solvothermal treatment, indicating that the solvothermal treatment had brought about a pure substitution reaction of the surface groups without any formation of TiO_2. The conclusions above are both in accordance with the results of XRD, Raman, and XPS total spectra mentioned earlier.

As for the influence of treating temperature, an obvious declining trend in the level of -OH groups could be observed in MN-1 to MN-3, and the proportion of -OH remained at a relatively low (but still higher than that of the untreated sample) level compared to MN-1 and MN-2. The increase in -OH groups after the solvothermal treatment should be attributed to the influence of H_2O. According to previous studies [21], the -OH groups are more likely to be oxidized to =O or even TiO_2 under a higher hydrothermal treating temperature. However, the reducibility of $NH_3 \cdot H_2O$ prevented MNSs from being oxidized to TiO_2, while partially hindering the transformation of -OH to =O. As a result, the amount

of -OH first rose to an extremely high value after the solvothermal treatment, then declined because of the oxidation when the temperature went higher. This effect is the most apparent between 40 °C and 80 °C; after that, the amount of -OH kept a relatively steady decrease, while seeing another noteworthily large decline from MN-7 to MN-8. For nanomaterials, the size effect has a non-negligible effect on the apparent properties. Among them, the degree of adsorbate-induced charge screening has an important influence on the critical size of the nanocrystal-lattice [22]. After the solvothermal treatment of the nanosheets, the -OH groups on the surface of the nanosheets increased, the strong charge screening effect reduced the critical size, and the size effect of the nanomaterials was weakened.

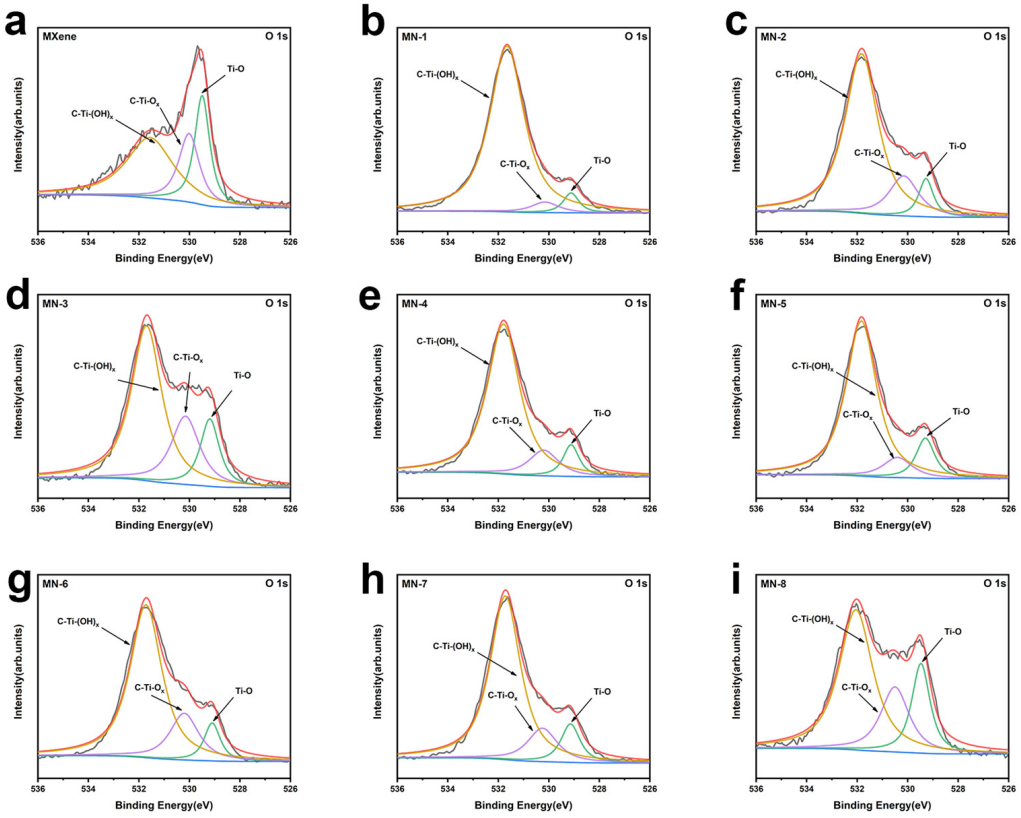


Figure 4. High-resolution XPS spectra of O 1s peaks of the MXene (**a**), MN-1 (**b**), MN-2 (**c**), MN-3 (**d**), MN-4 (**e**), MN-5 (**f**), MN-6 (**g**), MN-7 (**h**), and MN-8 (**i**) samples. Of these, the black line is the original spectrum, the red line is the fitted spectrum, the yellow line is the C-Ti-$(OH)_x$ bond spectrum, the purple line is the C-Ti-O_x bond spectrum, the green line is the Ti-O bond spectrum, and the blue line is the baseline.

Table 2. XPS statistics of the peak position and the area ratio of O 1s peaks.

Samples	Treating Temperature/°C	Position/eV			Area Ratio (α)		
		Ti-O	C-Ti-O_x	C-Ti-$(OH)_x$	[(C-Ti-O_x) + (C-Ti-$(OH)_x$)]/(Ti-O)	(C-Ti-$(OH)_x$)/(Ti-O)	(C-Ti-(OH)x)/[(C-Ti-Ox) + (Ti-O)]
MXene	-	529.55	530.30	531.80	2.57	1.71	0.92
MN-1	40	529.12	530.15	531.66	19.35	18.42	9.53
MN-2	60	529.26	530.15	531.82	11.53	9.43	3.05
MN-3	80	529.19	530.15	531.70	5.14	3.64	1.45
MN-4	100	529.12	530.20	531.79	10.96	9.48	3.82
MN-5	120	529.30	530.40	531.83	7.12	6.33	3.53
MN-6	140	529.10	530.20	531.72	10.16	7.94	2.47
MN-7	160	529.14	530.25	531.72	8.14	6.79	2.89
MN-8	180	529.47	530.50	532.04	4.00	2.87	1.35

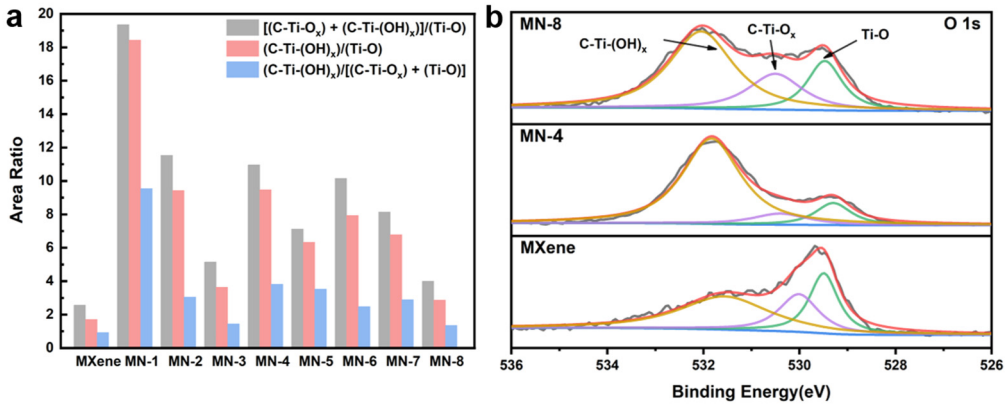


Figure 5. Area ratio between the differentiated peaks (**a**), and comparisons between the high-resolution spectra of O 1s of untreated MNSs, MN-5, and MN-8 (**b**). In (**b**), the black line is the original spectrum, the red line is the fitted spectrum, the yellow line is the C-Ti-$(OH)_x$ bond spectrum, the purple line is the C-Ti-O_x bond spectrum, the green line is the Ti-O bond spectrum, and the blue line is the baseline.

SEM and TEM were performed for MN-4 and MN-8, respectively, and the results are shown in Figure 6. As can be seen from the SEM images (Figure 6a,b), both MN-4 and MN-8 showed a wrinkled shape, which is different from the flat MXene morphology in Figure 1a. This is because the substitution of oxygen-containing functional groups to fluorine-containing functional groups on the surface of MXene during the $NH_3 \cdot H_2O$ solvent heat treatment resulted in the change in surface functional group states, and the different functional group steric hindrance resulted in the change in morphology. In addition, the increase in the number of electronegative functional groups on the surface led to the MXene nanosheets being able to adsorb more positive ions, leading to the formation of wrinkled surface morphology. It can be seen from the TEM images (Figure 6c,d) that when the temperature rose to 180 °C, incomplete grains were initially formed on the surface of MN-8, which also proved that high temperature oxidation, which leads to the reduction in surface functional groups and the formation of grains, plays a major role at high temperature.

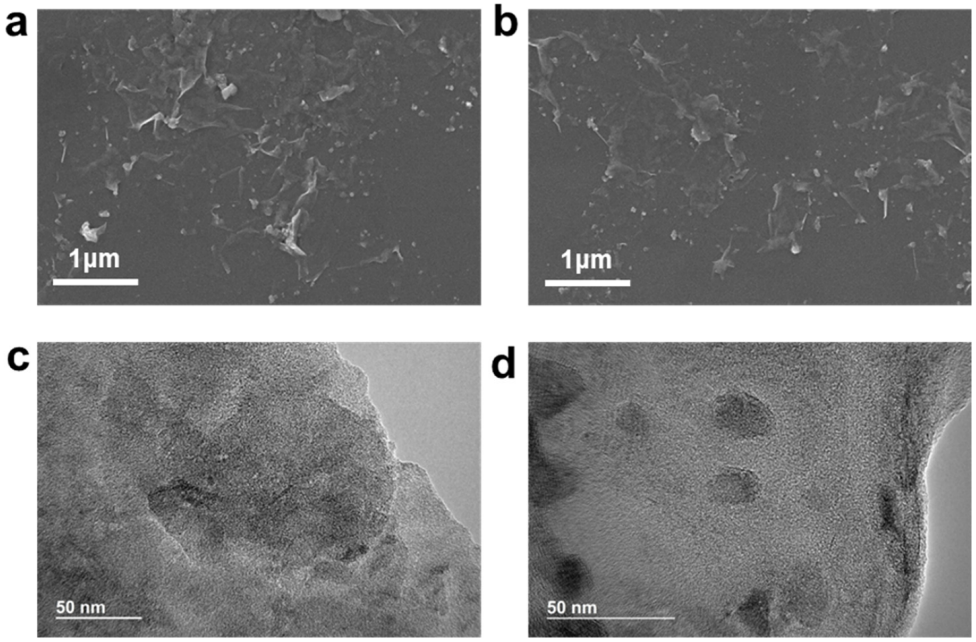


Figure 6. The SEM images of MN-4 (**a**) and MN-8 (**b**); the TEM images of MN-4 (**c**) and MN-8 (**d**).

The dielectric performances of the MNSs before and after $NH_3 \cdot H_2O$ solvothermal treatment were characterized in the form of an MNSs/paraffin composite using the coaxial method. The results are provided in Figure 7. Generally, the dielectric properties of MNSs are affected by the surface composition and morphology, as the surface functional groups and their positional relationship decide the number and efficiency of the ion polarization channels of MNSs, which significantly enhances the dielectric permittivity of the composite.

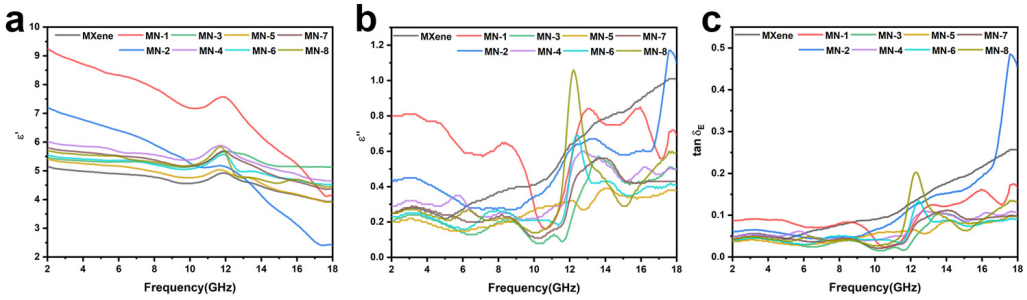


Figure 7. The dielectric performances of MNSs: the real part (**a**), the imaginary part (**b**) and the dielectric loss (**c**).

When the electromagnetic wave is incident on the surface of material, the polarization form caused by the electromagnetic wave determines the dielectric constant of the material, and the level of the dielectric constant determines the energy storage capacity. In low frequency regions, the polarization of particles such as grains and ions can respond to the change of electromagnetic waves, and then the polarization relaxation occurs, causing the change of dielectric constant. However, in the high-frequency region, large-size particles have no time to respond to the changes in electromagnetic waves, and the polarization is mainly manifested as the polarization of electrons. It can be seen that the real parts of the dielectric properties (dielectric permittivity) of the MNSs after the solvothermal treatment were higher than those of the untreated sample, while as the treating temperature went higher, the enhancement of the dielectric permittivity became slighter. MN-1 and MN-2 showed especially high low-frequency dielectric permittivity. The extents of the increase in dielectric permittivity were consistent with the amount change of surface -OH groups according to XPS characterization. The amount of -OH groups increased after solvothermal treatment and gradually decreased as the treatment temperature rose. The real parts of the dielectric properties of the samples shared the same changing trend as the -OH amount, indicating that surface -OH contributed the most to the ion polarization effect by providing more active ion polarization channels. In addition, the dielectric permittivity quickly declined to an ordinary level when the frequency moved to over 12 GHz. This is attributed to the domination of electron polarization in the dielectric permittivity, so that the enhancement of ion polarization made a relatively ignorable contribution to the dielectric permittivity. Since there is no oxide grain generation, the electromagnetic wave loss caused by ion polarization is relatively small. In this work, a 30% mass fraction composite material was prepared using paraffin as the matrix and treated nanosheets as the dopant, and its electromagnetic parameters were measured. For all MXene and MN-1-8 samples, the mass fraction of the paraffin matrix was 70%, so the change in dielectric constant was mainly caused by the MN nanosheets. For MN-1, the -OH group increased significantly after the $NH_3 \cdot H_2O$ solvent heat treatment, resulting in an enhanced low-frequency dielectric response and a significant increase in the dielectric constant in the low-frequency region. The large increase in the -OH group was mainly the substitution of -F group, both of which have a unit negative charge, and the overall electronic state of MXene nanosheets did not change significantly. Therefore, in the high-frequency region, the dielectric response caused by electron polarization did not change significantly, and the dielectric constant was basically the same as that of the original MXene. On the whole, the permittivity decreased rapidly from the low frequency region to the high frequency region.

According to Figure 7c, the imaginary parts and the dielectric loss (tan δ_E) showed no obvious change after the solvothermal treatment. In view of the effect of sheet stacking [23,24], we recorded statistics regarding the thickness distribution of the samples, and the specific methods were as follows: the AFM was used to test the thickness of the samples, and 20 representative nanosheets were selected for thickness statistics for each sample. After the statistical analysis of the results, the thickness of the nanosheets of all the samples after solvothermal treatment was between 2 and 5 nm, which was not significantly changed in comparison with MXene. This is also consistent with the XRD results. Since there was no doping of additional cations, the phenomenon of adsorption stacking between MXene nanosheets did not occur, so the change in dielectric constant had no obvious correlation with the stacking of the sheets.

4. Conclusions

In summary, $NH_3 \cdot H_2O$ solvothermal treatment was performed on $Ti_3C_2T_x$ MXene nanosheets (MNSs) at a temperature range between 40 °C to 180 °C, and the change in their surface compositions and dielectric performances were studied. Because of the reducibility of $NH_3 \cdot H_2O$, the MNSs were not oxidized to TiO_2. XRD and Raman spectra have proven the structural stability of MNSs under $NH_3 \cdot H_2O$ solvothermal treatment. In addition, obvious changes in the surface functional groups were discovered via the XPS survey and high-resolution spectra of the O 1s peaks. After the solvothermal treatment, a huge amount of -OH was grafted on the surface of MNSs, mainly replacing the positions of -F. When the treatment temperature was 100 °C, the optimal effect was achieved by replacing the fluorine-containing functional groups with oxygen-containing functional groups on the MXene surface. However, as the temperature went higher, although the oxidation of $Ti_3C_2T_x$ was hindered by reductive $NH_3 \cdot H_2O$, the -OH groups tended to be oxidized to =O. Combined with the destruction of surface functional groups by high temperatures, -OH declined to an amount that was just slightly higher than that of the untreated sample.

The change in the composition of surface functional groups had an impact on the dielectric properties of MNSs. After solvothermal treatment, the increased -OH provided more effective ion polarization channels to largely enhance the low-frequency dielectric permittivity of MNSs. The changing trend of the dielectric permittivity of the samples was consistent with the amount change of -OH groups, further verifying the conclusion that the -OH groups dominated the low-frequency dielectric behavior through the ion polarization effect. High dielectric permittivity and low dielectric loss are beneficial to its application in energy storage, electromagnetic wave shielding, etc. The clarification of the mechanics by which the surface groups influence the dielectric properties of MNSs and the preparation of MNSs with high intrinsic dielectric permittivity provide broader application areas in electronic devices for MXene-based materials.

Author Contributions: Conceptualization, Z.L. and G.L.; methodology, Z.L.; software, G.L.; validation, Z.L., G.L. and Y.Z.; formal analysis, Z.L. and G.L.; investigation, Z.L. and G.L.; resources, G.L.; data curation, Z.L. and G.L.; writing—original draft preparation, Z.L. and G.L.; writing—review and editing, Y.Z.; visualization, Z.L. and G.L.; supervision, X.C.; project administration, Z.L.; funding acquisition, Y.Z. All authors have read and agreed to the published version of the manuscript.

Funding: This research received no external funding.

Data Availability Statement: The data presented in this study are available on request from the corresponding author.

Conflicts of Interest: The authors declare no conflict of interest.

References

1. Kumar, A.; Yaduvanshi, R.S. Nano Spherical Dielectric Resonator Antenna for Rectenna Application. *Wirel. Pers. Commun.* **2023**, *128*, 161–172. [CrossRef]
2. Su, T.; Ma, X.; Tong, J.; Ji, H.; Qin, Z.; Wu, Z. Surface engineering of MXenes for energy and environmental applications. *J. Mater. Chem. A* **2022**, *10*, 10265–10296. [CrossRef]

3. Xu, X.; Chen, J.; Li, B. Phonon thermal conduction in novel 2D materials. *J. Phys. Condens. Matter* **2016**, *28*, 483001. [CrossRef]
4. Fu, Z.; Wang, N.; Legut, D.; Si, C.; Zhang, Q.; Du, S.; Germann, T.C.; Francisco, J.S.; Zhang, R. Rational Design of Flexible Two-Dimensional MXenes with Multiple Functionalities. *Chem. Rev.* **2019**, *119*, 11980–12031. [CrossRef] [PubMed]
5. Yang, J.; Bao, W.; Jaumaux, P.; Zhang, S.; Wang, C.; Wang, G. MXene-Based Composites: Synthesis and Applications in Rechargeable Batteries and Supercapacitors. *Adv. Mater. Interfaces* **2019**, *6*, 1802004. [CrossRef]
6. Li, Z.; Wang, Z.; Lu, W.; Hou, B. Theoretical Study of Electromagnetic Interference Shielding of 2D MXenes Films. *Metals* **2018**, *8*, 652. [CrossRef]
7. Lin, L.; Sherrell, P.; Liu, Y.; Lei, W.; Zhang, S.; Zhang, H.; Wallace, G.G.; Chen, J. Engineered 2D Transition Metal Dichalcogenides—A Vision of Viable Hydrogen Evolution Reaction Catalysis. *Adv. Energy Mater* **2020**, *10*, 1903870. [CrossRef]
8. Wang, Q.; O'Hare, D. Recent Advances in the Synthesis and Application of Layered Double Hydroxide (LDH) Nanosheets. *Chem. Rev.* **2012**, *112*, 4124–4155. [CrossRef]
9. Khan, U.; May, P.; O'Neill, A.; Bell, A.P.; Boussac, E.; Martin, A.; Semple, J.; Coleman, J.N. Polymer reinforcement using liquid-exfoliated boron nitride nanosheets. *Nanoscale* **2013**, *5*, 581–587. [CrossRef]
10. Xiao, X.; Song, H.; Lin, S.; Zhou, Y.; Zhan, X.; Hu, Z.; Zhang, Q.; Sun, J.; Yang, B.; Li, T.; et al. Scalable salt-templated synthesis of two-dimensional transition metal oxides. *Nat. Commun.* **2016**, *7*, 11296. [CrossRef]
11. Xiao, X.; Yu, H.; Jin, H.; Wu, M.; Fang, Y.; Sun, J.; Hu, Z.; Li, T.; Wu, J.; Huang, L.; et al. Salt-Templated Synthesis of 2D Metallic MoN and Other Nitrides. *ACS Nano* **2017**, *11*, 2180–2186. [CrossRef] [PubMed]
12. Shahzad, F.; Iqbal, A.; Kim, H.; Koo, C.M. 2D Transition Metal Carbides (MXenes): Applications as an Electrically Conducting Material. *Adv. Mater.* **2020**, *32*, 2002159. [CrossRef] [PubMed]
13. Lukatskaya, M.R.; Mashtalir, O.; Ren, C.E.; Dall'Agnese, Y.; Rozier, P.; Taberna, P.L.; Naguib, M.; Simon, P.; Barsoum, M.W.; Gogotsi, Y. Cation intercalation and high volumetric capacitance of two-dimensional titanium carbide. *Science* **2013**, *341*, 1502–1505. [CrossRef]
14. VahidMohammadi, A.; Rosen, J.; Gogotsi, Y. The world of two-dimensional carbides and nitrides (MXenes). *Science* **2021**, *372*, 6547. [CrossRef] [PubMed]
15. Ghidiu, M.; Lukatskaya, M.R.; Zhao, M.; Gogotsi, Y.; Barsoum, M.W. Conductive two-dimensional titanium carbide 'clay' with high volumetric capacitance. *Nature* **2014**, *516*, 78–81. [CrossRef]
16. Kamysbayev, V.; Filatov, A.S.; Hu, H.; Xue, R.; Lagunas, F.; Wang, D.; Klie, R.F.; Talapin, D.V. Covalent surface modifications and superconductivity of two-dimensional metal carbide MXenes. *Science* **2020**, *369*, 979–983. [CrossRef]
17. Lim, K.R.G.; Handoko, A.D.; Nemani, S.K.; Wyatt, B.; Jiang, H.; Tang, J.; Anasori, B.; Seh, Z.W. Rational Design of Two-Dimensional Transition Metal Carbide/Nitride (MXene) Hybrids and Nanocomposites for Catalytic Energy Storage and Conversion. *ACS Nano* **2020**, *14*, 10834–10864. [CrossRef]
18. Tang, Q.; Zhou, Z.; Shen, P. Are MXenes Promising Anode Materials for Li Ion Batteries? Computational Studies on Electronic Properties and Li Storage Capability of Ti_3C_2 and $Ti_3C_2X_2$(X = F, OH) Monolayer. *J. Am. Chem. Soc.* **2012**, *134*, 16909–16916. [CrossRef]
19. Tu, S.; Jiang, Q.; Zhang, J.; He, X.; Hedhili, M.N.; Zhang, X.; Alshareef, H.N. Enhancement of Dielectric Permittivity of $Ti_3C_2T_x$ MXene/Polymer Composites by Controlling Flake Size and Surface Termination. *ACS Appl. Mater. Interfaces* **2019**, *11*, 27358–27362. [CrossRef]
20. Guo, J.; Peng, Q.; Fu, H.; Zou, G.; Zhang, Q. Heavy-Metal Adsorption Behavior of Two-Dimensional Alkalization-Intercalated MXene by First-Principles Calculations. *J. Phys. Chem. C* **2015**, *119*, 20923–20930. [CrossRef]
21. Persson, I.; Halim, J.; Hansen, T.W.; Wagner, J.B.; Darakchieva, V.; Palisaitis, J.; Rosen, J.; Persson, P.O.Å. How Much Oxygen Can a MXene Surface Take Before It Breaks. *Adv. Funct. Mater.* **2020**, *30*, 1909005. [CrossRef]
22. Yasui, K.; Kato, K. Influence of Adsorbate-Induced Charge Screening, Depolarization Factor, Mobile Carrier Concentration, and Defect-Induced Microstrain on the Size Effect of a $BaTiO_3$ Nanoparticle. *J. Phys. Chem. C* **2013**, *117*, 19632–19644. [CrossRef]
23. Andersen, K.; Latini, S.; Thygesen, K.S. Dielectric Genome of van der Waals Heterostructures. *Nano Lett.* **2015**, *15*, 4616–4621. [CrossRef] [PubMed]
24. Tian, T.; Scullion, D.; Hughes, D.; Li, L.H.; Shih, C.-J.; Coleman, J.N.; Chhowalla, M.; Santos, E.J.G. Electronic Polarizability as the Fundamental Variable in the Dielectric Properties of Two- Dimensional Materials. *Nano Lett.* **2020**, *20*, 841–851. [CrossRef]

Disclaimer/Publisher's Note: The statements, opinions and data contained in all publications are solely those of the individual author(s) and contributor(s) and not of MDPI and/or the editor(s). MDPI and/or the editor(s) disclaim responsibility for any injury to people or property resulting from any ideas, methods, instructions or products referred to in the content.